



LAWRENCE
LIVERMORE
NATIONAL
LABORATORY

The Community Climate System Model: CCSM3

W. D. Collins, M. Blackmon, C. Bitz, G. Bonan, C. S.
Bretherton, J. A. Carton, P. Chang, S. Doney, J. J.
Hack, J. T. Kiehl, T. Henderson, W. G. Large, D.
McKenna, B. D. Santer, R. D. Smith

December 29, 2004

Journal of Climate

Disclaimer

This document was prepared as an account of work sponsored by an agency of the United States Government. Neither the United States Government nor the University of California nor any of their employees, makes any warranty, express or implied, or assumes any legal liability or responsibility for the accuracy, completeness, or usefulness of any information, apparatus, product, or process disclosed, or represents that its use would not infringe privately owned rights. Reference herein to any specific commercial product, process, or service by trade name, trademark, manufacturer, or otherwise, does not necessarily constitute or imply its endorsement, recommendation, or favoring by the United States Government or the University of California. The views and opinions of authors expressed herein do not necessarily state or reflect those of the United States Government or the University of California, and shall not be used for advertising or product endorsement purposes.

The Community Climate System Model: CCSM3

**William D. Collins^{1*}, Maurice Blackmon¹, Cecilia Bitz², Gordon Bonan¹,
Christopher S. Bretherton², James A. Carton³, Ping Chang⁴, Scott Doney⁵,
James J. Hack¹, Jeffrey T. Kiehl¹, Thomas Henderson¹, William G. Large¹,
Daniel McKenna¹, Benjamin D. Santer⁶, and Richard D. Smith⁷**

¹ National Center for Atmospheric Research, Boulder, Colorado 80307

² University of Washington, Seattle Washington 98195

³ University of Maryland, College Park, Maryland 20742

⁴ Texas A&M University, College Station, Texas 77843

⁵ Woods Hole Oceanographic Institution, Woods Hole, Massachusetts 02543

⁶ Lawrence Livermore National Laboratory, Livermore, California 94551

⁷ Los Alamos National Laboratory, Los Alamos, New Mexico 87545

December 3, 2004

Abstract

A new version of the Community Climate System Model (CCSM) has been developed and released to the climate community. CCSM3 is a coupled climate model with components representing the atmosphere, ocean, sea ice, and land surface connected by a flux coupler. CCSM3 is designed to produce realistic simulations over a wide range of spatial resolutions, enabling inexpensive simulations lasting several millenia or detailed studies of continental-scale climate change. This paper will show results from the configuration used for climate-change simulations with a T85 grid for atmosphere and land and a 1-degree grid for ocean and sea-ice. The new system incorporates several significant improvements in the scientific formulation. The enhancements in the model physics are designed to reduce or eliminate several systematic biases in the mean climate produced by previous editions of CCSM. These include new treatments of cloud processes, aerosol radiative forcing, land-atmosphere fluxes, ocean mixed-layer processes, and sea-ice dynamics. There are significant improvements in the sea-ice thickness, polar radiation budgets, equatorial sea-surface temperatures, ocean currents, cloud radiative effects, and ENSO teleconnections. CCSM3 can produce stable climate simulations of millennial duration without ad hoc adjustments to the fluxes exchanged among

*NCAR, P.O. Box 3000, Boulder, CO. 80307, email: wcollins@ucar.edu

the component models. Nonetheless, there are still systematic biases in the ocean-atmosphere fluxes in western coastal regions, the spectrum of ENSO variability, the spatial distribution of precipitation in the Pacific and Indian Oceans, and the continental precipitation and surface air temperatures. We conclude with the prospects for extending CCSM to a more comprehensive model of the Earth's climate system.

1. Introduction

The Community Climate System Model (CCSM) is a coupled model for simulating past, present, and future climates. In its present form, CCSM consists of four components for the atmosphere, ocean, cryosphere and land surface linked through a coupler that exchanges fluxes and state information among these components. It is developed and used by an international community of students and scientists from universities, national laboratories, and other institutions. Applications include studies of interannual and interdecadal variability, simulations of paleoclimate regimes, and projections of future anthropogenic climate change for international assessments. The most recent version, CCSM3, has been released to the climate community on 23 June, 2004. This paper describes some of the most important advances in model physics and dynamics, improvements in the simulated climate, and remaining scientific challenges for future development of CCSM.

CCSM3 is the third generation in an ongoing series of coupled models developed through international collaboration. The first generation, the Climate System Model version 1 (CSM-1), was released in 1996 (Boville and Gent 1998). This model was noteworthy since it did not require adjustments to the fluxes exchanged among the physical components in order to simulate stable, relatively drift-free climates. The second generation, the Community Climate System Model version 2 (CCSM2), was released in 2002 (Kiehl and Gent 2003). The climate simulated with CCSM2 exhibited several improvements over the climate generated from CSM1. The new model produced better simulations of extratropical sea surface temperatures, better tropical variability, and more realistic land surface temperatures. However, several important deficiencies prompted a new cycle of development that has resulted in CCSM3. The main model biases in CCSM2 include a double ITCZ and extended cold tongue; overestimation of winter land surface temperatures; underestimation of of tropical tropopause temperatures; erroneous cloud response to SST changes; errors in the east Pacific surface energy budget; and underestimation of tropical variability. As we will show, the new model has reduced or eliminated some of these biases.

This overview and the subsequent papers will focus on a configuration of CCSM with atmosphere and land models on Eulerian spatial grids T85 spectral truncation and ocean and sea-ice models with 1-degree lateral resolution at the equator (Appendix A). This configuration has been applied to simulations for international climate-change assessments. Lower-resolution versions of CCSM have been developed for applications including rapid scientific development, simulations of biogeochemical processes requiring multi-century simulations for equilibration, and studies of deep-time paleoclimate regimes. The sensitivity of the simulated climate to model resolution is discussed

67 in Hack and Etcetera (2004), Yeager et al. (2004), Otto-Bliesner et al. (2004), and
68 DeWeaver and Bitz (2004).

69 Basic features of the mean climate and its stability are discussed in this paper. De-
70 tailed analyses of the variability and transient behavior of the systems are presented in
71 Deser et al. (2004), Alexander et al. (2004), Meehl et al. (2004), and Gent et al. (2004).
72 Major improvements in the component models are outlined in section 2. Thorough
73 descriptions of the enhancements in individual components are given elsewhere in this
74 special issue (Collins et al. 2004b; Large et al. 2004, e.g.,). Improvements in the cli-
75 mate simulation and reductions in systematic errors relative to CCSM2 are discussed
76 in section 3. The stability of the mean climate and analysis of secular trends in climate
77 parameters are presented in section 4. Some of the most significant challenges for im-
78 proving the simulations in future versions of CCSM are discussed in section 5. Plans
79 for further development and extension to coupled chemistry-climate applications are
80 presented in section 6.

81 **2. Overview of CCSM3**

82 The CCSM3.0 system includes new versions of all the component models. The model
83 versions are CAM version 3.0 (Collins et al. 2004c,b), CLM version 3.0, CSIM ver-
84 sion 5.0 (Briegleb et al. 2004), and POP version 1.4.3. New features in each of these
85 components are described below.

86 **a. *Design for multiple resolutions and atmospheric dynamics***

87 CCSM3 has been designed to produce simulations with reasonable fidelity over a wide
88 range of resolutions and with a variety of atmospheric dynamical frameworks. This
89 is accomplished by introducing dependence on resolution and dynamics in the time
90 step and twelve other adjustable parameters in CAM3 (Collins et al. 2004c). With one
91 exception, those parameters affect the physics governing clouds and precipitation in
92 the atmosphere.

93 The standard version of CAM3 is based upon the Eulerian spectral dynamical core
94 with triangular spectral truncation at 31, 42, and 85 wavenumbers. The zonal resolution
95 at the equator ranges from 3.75° to 1.41° for the T31 and T85 configurations. It is also
96 possible to integrate CCSM3 with a finite-volume dynamical core (Lin and Rood 1996,
97 1997) at 2 by 2.5-degree resolution, although at present this variant of CCSM3 is an
98 experimental version requiring further refinement. The vertical dimension is treated
99 using 26 levels with a hybrid coordinate. The land model is integrated on the same
100 horizontal grid as the atmosphere, although each grid box is further divided into a
101 hierarchy of land units, ground cover, and plant types. There are ten sub-surface soil
102 layers in CLM3.

103 The ocean model uses a dipole grid with a horizontal resolution of 3° or 1° . The
104 semi-analytic grids have the first pole located at the true South Pole and the second
105 pole located over north America (Smith et al. 1995). The vertical dimension is treated
106 using a height (z) coordinate with 25 levels extending to 4.75 in the 3-degree version
107 and 40 levels extending to 5.37 km in the 1-degree version. The sea-ice model shares

108 the same grid with the ocean model.

109 The three standard configurations CAM combine the T31 CAM/CLM with the 3°
110 POP/CSIM, the T42 CAM/CLM with the 1° POP/CSIM, and the T85 CAM/CLM with
111 the 1° POP/CSIM.

112 **b. *Development the Atmosphere Component***

113 The new atmospheric model includes significant changes to the dynamics, cloud and
114 precipitation processes, radiation processes, and treatments of aerosols. The finite vol-
115 ume dynamical core is now included as a standard option for integrating CAM (Boville
116 et al. 2004). The tendency equations can be integrated with either process-split or time-
117 split formulations of the numerical difference approximations (Williamson 2002). The
118 physics of cloud and precipitation processes has been modified extensively (Boville
119 and Etcetera 2004). The modifications include separate treatments of liquid and ice
120 condensate; advection, detrainment, and sedimentation of cloud condensate; and sep-
121 arate treatments of frozen and liquid precipitation. The radiation has been updated
122 with a generalized treatment of cloud geometrical overlap (Collins et al. 2001) and
123 new treatment of longwave and shortwave interactions with water vapor (Collins et al.
124 2002a, 2004a). The prognostic sulfur cycle developed by Barth et al. (2000); Rasch
125 et al. (2000) for predicting sulfate aerosols is now a standard option for the model. A
126 prescribed distribution of sulfate, soil dust, carbonaceous species, and sea salt based
127 upon a three-dimensional assimilation (Collins 2001; Rasch et al. 2001) is used to
128 calculate the direct effects of tropospheric aerosols on the heating rates (Collins et al.
129 2002b). The corresponding effects of stratospheric volcanic aerosols are parameterized
130 following (Ammann et al. 2003).

131 **c. *Development of the Ocean Component***

132 The new ocean model includes modifications to the boundary layer physics and the
133 numerical techniques for solving the barotropic continuity equations. The most sig-
134 nificant modification is the inclusion of solar heating by chlorophyll based upon the
135 parameterization by Ohlmann (2004). Transmissions vary spatially and are updated
136 monthly. In contrast with the spatially uniform transmission factors used in CCSM2.0,
137 subtropical oceans far from land are generally more transmissive while mid-latitude,
138 coastal, and equatorial oceans are less transmissive. There are also minor modifica-
139 tions to the viscosities and diffusivities used in the K-profile parameterization (KPP)
140 for vertical ocean mixing. In distinction with previous generations of CCSM, double
141 diffusion associated with salt fingering is included by default in CCSM3.0. Air-sea
142 exchanges of momentum, sensible heat, and latent heat are computed using the relative
143 wind speed equal to the magnitude of the vector difference between the near-surface
144 wind and the ocean surface currents. Finally the numerical algorithm for solving the
145 barotropic equation has been replaced with a more efficient method to accelerate the
146 computational performance of the ocean code.

147 **d. *Development of the Land Component***

148 One of the primary objectives of the land developers has been to reduce the positive
149 continental temperature biases during boreal winter. Modifications to the relationship
150 between snow height and equivalent water depth, which have a significant impact on
151 land-surface albedos (Oleson et al. 2003), have been considered but have not been
152 adopted in CCSM3. The major change to the formulation of the biogeophysics in-
153 creases the sensible and latent heat fluxes over vegetated surfaces. In previous versions
154 of CCSM, the turbulent transfer coefficient between soil and the overlying canopy air
155 was a constant for dense canopies. The new formulation makes this coefficient de-
156 pendent on canopy density characterized by leaf and stem area indices (Oleson et al.
157 2004).. The transfer coefficient is used to obtain aerodynamic resistances for heat and
158 moisture which are used to compute latent and sensible heat fluxes. Over large areas
159 of Eurasia, these changes results in a reduction of the 2-meter air temperature by -1.5
160 to -2 K.

161 The new land model is based upon a nested subgrid hierarchy of scales representing
162 land units, soil or snow columns, and plant functional types (PFTs) (Bonan et al. 2001;
163 Oleson et al. 2004). CCSM3.0 includes the effects of competition for water among
164 PFTs in its standard configuration.

165 **e. *Development of the Sea-Ice Component***

166 The CSIM includes modifications to the formulation of ice dynamics, sea-ice albe-
167 dos, and exchanges of salt between sea-ice and the surrounding ocean. The horizon-
168 tal advection of sea ice is now treated with incremental remapping, a more accurate
169 and efficient scheme than that used in previous versions(Libscomb and Hunke 2004).
170 The momentum equation has been modified using scaling arguments to better simulate
171 marginal ice under free drift (Connolley et al. 2004). The ice albedos have been em-
172 pirically adjusted to yield better seasonal cycles of snow cover in the Arctic basin. The
173 adjusted albedos are generally lower than the values adopted in CCSM2.0, although
174 both sets of albedos are consistent with the ranges of observational estimates. The
175 adjustments improve the rapid reduction in surface reflectivity during Arctic spring as-
176 sociated with snow melt. Exchange of sea salt with ocean water is included for ice melt,
177 net congelation at ice base, net sublimation and condensation, and snow ice formation.

178 **3. The mean coupled climate**

179 There have been several significant improvements in the climate produced by CCSM3
180 relative to the climate simulated by CCSM2. These improvements are evident in a
181 comparison of the control integrations of the two models for present-day conditions.
182 In these comparisons, the mean climate produced by CCSM2 is represented by the
183 average of years 900 to 1000 of its control simulation. This time period includes the
184 interval that Kiehl and Gent (2003) used to describe the climate of CCSM2. For the
185 CCSM2 control, the atmosphere and land are run at T42 resolution while the ocean and
186 sea-ice are on a 1° grid. The mean climate produced by CCSM3 is represented by the
187 average of years 400 to 500 from a control simulation using the model at its highest

standard resolution (Appendix A). This time period is the same interval evaluated by Hurrell and Etcetera (2004). The comparison between the two integrations can change with time due to the secular trends in both runs (section 4 and Kiehl and Gent (2003)). However, the trends are sufficiently small that the major differences in, for example, sea-surface temperature are not appreciably affected.

a. Energy balance at the surface and top of model

The most significant change in radiation budget of CCSM3 is the disposition of solar radiation in the atmosphere. The atmosphere in CCSM3 absorbs 7.1 Wm^{-2} more shortwave radiation in clear-sky conditions and 7.9 Wm^{-2} more under all-sky conditions. The increased absorption is caused primarily the introduction of absorbing aerosol species (section b) and the updates to the extinction of near-infrared radiation by water vapor. The new aerosols increase the absorption by 2.8 Wm^{-2} for both clear-sky and all-sky conditions. The new treatment of near-infrared extinction by H_2O increases the clear and all-sky atmospheric absorption by 4.0 and 3.1 Wm^{-2} , respectively. The enhanced absorption reduces the surface insolation by an equal amount. As a result, the net surface shortwave flux in CCSM3 is 9 Wm^{-2} smaller than that in CCSM2 (Figure 1). The new annual mean insolation of 160 Wm^{-2} is consistent with several empirical estimates (Kiehl and Trenberth 1997), although it is lower than the most recent ISCCP value of 166 Wm^{-2} (Zhang et al. 2004). Some of the largest discrepancies between model and ISCCP calculations occur in the tropics, where ISCCP overestimates the all-sky downwelling flux by 21 Wm^{-2} compared to surface radiometers.

Figure 1

The fidelity of the shortwave cloud forcing in CCSM3 to estimates from the Earth Radiation Budget Experiment (Harrison et al. 1990)¹ has improved, especially in the storm tracks. CCSM2 underestimated the magnitude of global annual-mean shortwave cloud forcing by 5.8 Wm^{-2} , while CCSM3 reproduces the ERBE estimates to within 0.1 Wm^{-2} . The largest zonal-mean differences occur in the storm tracks at 60N and 60S and in the tropical ITCZ between 10N and 10S . The increased forcing is in better agreement with the satellite data for the storm tracks and in slightly worse agreement for the tropics.

The all-sky and clear-sky surface longwave fluxes have decreased by 6.9 Wm^{-2} and 7.5 Wm^{-2} . The reductions in clear-sky flux in polar regions are related to the new longwave parameterization for water vapor (Collins et al. 2002a). These changes bring the model into much better agreement with in situ observations (Briegleb and Bromwich 1998).

b. Sea surface temperature and salinity

Several of the systematic errors in SSTs in CCSM2 have been reduced in CCSM3. Earlier versions of CCSM have consistently generated a region of equatorial water in the eastern Pacific which is colder than observed and extends too far west into the warm pool. The SSTs in this region have increased by between 1K and 2K in the central and

228 western Pacific (Figure 2). A substantial fraction² of the SST increased is caused by
229 the revisions to solar absorption by chlorophyll in the ocean mixed layer. The cold SST
230 bias in the central equatorial Pacific exceeded 2K in CCSM2, and it is less than 1K in
231 CCSM3. The equatorial SSTs in the warm pool are underestimated by between 0.2 to
232 0.5K.

Figure 2

233 The CCSM2 also overestimates the SSTs by as much as 5K in narrow coastal re-
234 gions just west of North and South America and southern Africa. This bias is not
235 eliminated in CCSM3, but the SST errors have decreased by between 1K and 2K west
236 of the American continents. The reductions in the biases result from better simulations
237 of the observed insolation and surface stress, which leads to more coastal upwelling
238 (section d).

239 The mean surface salinity errors in CCSM3 are -0.40 psu, a slight improvement
240 over the corresponding error of -0.43 psu in CCSM2. One of the major areas of
241 improvement is the equatorial surface salinity in the Pacific. In CCSM2, the western
242 edge of the warm pool is two fresh by up to 2 psu³, while the eastern edge too fresh
243 by 0.5 to 1 psu. In CCSM3, the biases at both edges have been halved⁴. However,
244 the equatorial Indian Ocean is too fresh by up to 2 psu, and the southern subtropical
245 Pacific is too fresh by up to 1.5 psu. The precipitation in both of these regions relative
246 to observations has increased from CCSM2 to CCSM3.

247 c. Oceanic heat transport

248 The meridional heat transport in CCSM3 is similar to the transports by mean flow
249 in CCSM2. The maximum heat transport in the northern hemisphere is 2.2 PW⁵,
250 close to the 2 PW peak simulated by CCSM2 and comparable to recent observations
251 (Kiehl and Gent 2003)(Figure 3). The maximum transport in the southern hemisphere
252 is approximately 0.6 PW, somewhat lower than the 0.85 PW produced by CCSM2.
253 In the southern hemisphere, the peak mean transport toward the equator is marginally
254 weaker in CCSM3 than CCSM2.⁶

Figure 3

255 d. Oceanic circulations

256 The representation of the equatorial Pacific undercurrent has improved in CCSM3. The
257 realism of the simulated current can be evaluated against current measurements from
258 the TOGA TAO buoy array (McPhaden et al. 1998). Previous versions of CCSM have
259 tended to underestimate the strength of the counter-current. In CCSM3, the velocity
260 at the core exceeds 100 cm/s, which is slightly larger than the velocities measured
261 from the array (Figure 4)⁷ The simulated counter-current is displaced downward by
262 XX m⁸, but otherwise its vertical and meridional extent are in good agreement with

Figure 4

¹line 211: The comparison is actually against Trenberth-modified ERBE – need reference

²line 228: How much of heating of equatorial Pacific is due to revision in chlorophyll heating?

³line 242: Estimate of CCSM2 surf. salinity bias at 120E

⁴line 243: What is the east-west gradient in salinity error in CCSM3?

⁵line 249: Verify maximum Eulerian mean NHT using years 400-499,

⁶line 254: Need figure for the section c from OS on ocean heat transport.

⁷line 261: Figure is for years 571-600: need to replace with average for years 400-500. Also, what is the longitude averaging range?

⁸line 262: What is the vertical displacement of the equa. Pac. c.c. relative to obs?

263 observations.

264 **e. Sea-ice thickness and concentration**

265 The fidelity of Arctic sea-ice thickness and distribution have improved in CCSM3 relative to earlier versions of the model. The annual mean ice thickness is between 2
266 and 2.5m over the central Arctic basin, with thicknesses exceeding 3m in the Beaufort
267 Sea (Figure 5)⁹. The measured sea-ice thickness ranges between 2–3m, and CCSM2
268 produced ice with a mean thickness of 1.5m. The high resolution version of CCSM3
269 reproduces the observed gradient in sea-ice thickness across the Arctic basin from the
270 east Siberian to Beaufort Seas (DeWeaver and Bitz 2004). The sea-ice concentration is
271 not significantly different from the concentrations simulated by CCSM2. Like CCSM2,
272 CCSM3 overestimates the concentrations in the Labrador Sea (Figure 5). Both the in-
273 termediate and high-resolution versions of CCSM3 produce excessive sea-ice in the
274 Sea of Okhotsk, although the bias is less manifest at the higher resolution. The ampli-
275 tudes of the seasonal cycle in northern hemisphere ice area simulated by the interme-
276 diate and high-resolution versions of CCSM3 are larger than observed. The simulated
277 summertime area of approximately $5 \times 10^6 \text{ km}^2$ is in good agreement with observa-
278 tions. However, in winter the modeled sea ice area of $1.5 \times 10^7 \text{ km}^2$ exceeds the
279 observed area of approximately $1.2 \times 10^7 \text{ km}^2$ (Weatherly et al. 1998).

Figure 5

281 In the southern hemisphere, the sea-ice produced by CCSM3 is slightly more exten-
282 sive than the ice area from CCSM2. Since CCSM2 produces a larger ice pack than ob-
283 served, the bias in surface area in CCSM3 is slightly worse. At the end of the CCSM3
284 control integration, the surface area is approximately $1.3 \times 10^7 \text{ km}^2$ while the observed
285 annual-mean surface area is approximately $1.0 \times 10^7 \text{ km}^2$. CCSM3 slightly overesti-
286 mates the observed austral summertime minimum in sea-ice area of $2.1 \times 10^6 \text{ km}^2$. In
287 the austral winter, the modeled maximum sea ice area of up to $2.0 \times 10^7 \text{ km}^2$ signifi-
288 cantly exceeds the observed maximum of $1.5 \times 10^7 \text{ km}^2$ (Weatherly et al. 1998). The
289 spatial distribution of sea-ice thickness, however, is in better agreement with the recent
290 observational estimates of Timmermann et al. (2004).

291 **f. Climate sensitivity**

292 Climate sensitivity is a measure of how a simulated climate changes in response to ex-
293 ternal forcing. In its traditional definition, climate sensitivity is the increase in global-
294 average annual-mean surface temperature when the atmospheric concentration of car-
295 bon dioxide is doubled. Although climate sensitivity is not a useful metric for regional
296 climate change, it has proven to be a very useful index for categorizing the response of
297 multi-model ensembles to a given climate-change scenario (IPCC 2001).

298 The equilibrium sensitivity of CCSM3 in its high-resolution configuration is $2.7 \pm$
299 $X \text{ K}$ for an increase from 355 to 710 ppmv (Kiehl et al. 2004). This represents an in-
300 crease of 23% over the equilibrium sensitivity of 2.2K for CCSM2 (Kiehl and Gent
301 2003). The two factors contributing to the increased sensitivity are the changes to the
302 cloud processes in CAM (section b) and the resolution-dependent tuning of the cloud
303 processes (section a). The climate sensitivity of CCSM3 increases with increasing res-

⁹line 268: Redo sea ice figures using years 400-500 rather than years 401-410.

304 olution of the atmosphere and land models. This variation is directed related to the
305 variation in cloud radiative feedbacks with resolution (Kiehl and Gent 2003).

306 **4. Stability and long-term behavior of coupled integra-** 307 **tion**

308 CCSM3 has been designed to provide stable simulation relatively free of secular trends
309 under fixed boundary conditions. The stability in the model system is a important
310 design objective for two reasons. First, the absence of large trends is a necessary but
311 not sufficient test of the conservation of energy, mass, and total water content of each
312 of the components. Second, drift-free simulations are required for some of the more
313 demanding applications of the model, including simulations of the carbon cycle that
314 require millenia to attain equilibrium. The stability can be addressed by examining the
315 energy budget and other properties of an integration for present-day conditions during
316 years 100 to 600 (Appendix A).

317 In order for the climate system to be in equilibrium, the exchange of radiative
318 energy across the top of the atmospheric model (TOM) must be as close to zero as
319 possible. The exchange of radiant energy is the difference between the net shortwave
320 radiation absorbed by the system and the net longwave radiation emitted by the system.
321 For CCSM3, the annual-mean and RMS TOM energy balance is $-0.21 \pm 0.28 \text{ Wm}^{-2}$.
322 Since the sign convention on the TOM balance is positive downward, on average the
323 CCSM3 loses energy under present-day conditions. This loss rate is nearly identical
324 to the loss rate of -0.2 Wm^{-2} for CCSM2 (Kiehl and Gent 2003). For compari-
325 son, the annual-mean net solar radiation absorbed at TOM under all-sky condition is
326 234.21 Wm^{-2} . The energy imbalance in the system is equivalent to 0.08% of the net
327 solar input. The TOM all-sky and clear-sky fluxes are relatively stable, with trends
328 between -0.01 and $-0.03 \text{ Wm}^{-2}/\text{century}$.

329 Similarly, equilibrium of the climate system requires that the global-mean surface
330 energy balance also be as close to zero as possible. The exchange of energy among
331 the atmosphere and surface components is the difference between the net downward
332 all-sky shortwave radiation, the net upward all-sky longwave radiation, the latent heat
333 flux, and the sensible heat flux. For CCSM3, the annual-mean and RMS surface energy
334 balance is $-0.23 \pm 0.21 \text{ Wm}^{-2}$. The net energy absorbed by the atmosphere is just
335 the difference between the TOM and surface energy balances. For CCSM3, the mean
336 and RMS energy absorbed by the atmosphere is $0.02 \pm 0.13 \text{ Wm}^{-2}$. The atmospheric
337 model includes a correction applied at each time step that sets the absorbed energy to
338 zero. In the absence of that correction, the time-mean global-average energy absorbed
339 is -0.27 Wm^{-2} . This residual absorption is due to numerical dissipation and to en-
340 ergy imbalances introduced by approximations related to water vapor and its phase
341 transformations.

342 Since the simulated climate system is slowly losing energy, the global mean surface
343 temperature should decrease slowly with time. After an initial 100-year period required
344 to equilibrate the Arctic sea ice, the surface temperature decreases by -0.011K per
345 century. Most of this trend is manifested in the southern hemisphere between 30S and

346 90S, which cools at a rate of -0.04K per century. The temperatures in the tropics
347 between 30S and 30N and the northern hemisphere between 30N and 90N increase by
348 less than $2 \times 10^{-4}\text{K}$ per century.

349 The trend in the global volume-mean ocean temperature is -0.05K per century
350 (Figure 6). As in CSM1 (Boville and Gent 1998)¹⁰, the initial ocean adjustment to the
351 energy imbalances at TOM occurs well below the mixed layer (Figure 7).

Figure 6

Figure 7

352 The decrease in the temperature of the southern hemisphere can be explained either
353 by the expansion of the southern sea-ice or by the persistent cooling of the deep ocean
354 water upwelling adjacent to Antarctica. The trends in sea-ice is in the northern and
355 southern hemispheres are -0.02×10^6 and $0.18 \times 10^6 \text{ km}^2$ per century, respectively.
356 These changes correspond to changes in ice concentration (expressed in percent) of
357 -0.002% and 0.015% per century. The temperature trend can be decomposed into a
358 sum of terms associated with the trends in the areas and temperatures of the southern
359 ocean, southern sea-ice, and ice over Antarctica. The decomposition shows that 83%
360 of the southern-hemisphere trend is determined by the increase in sea-ice area and the
361 -18.6K temperature differential between the sea-ice and surrounding ocean.

362 The trend in the global volume-mean salinity is $-6.2 \times 10^{-5} \text{ psu/century}$. Com-
363 pared to the global mean salinity of 34.72 psu, the trend in salinity is equivalent to a
364 relative change of $-2 \times 10^{-4}\%$ per century. This reduction in salinity is caused by the
365 adjustment of the soil moisture in the deepest layers of the land model during the first
366 300 years of integration (Kiehl and Gent 2003). Excess deep soil moisture is gradu-
367 ally released to the oceans by river runoff. These trends are smaller in magnitude, but
368 opposite in sign, to the changes in salinity in CCSM2 (Kiehl and Gent 2003).

369 5. Challenges for further development

370 While many features of the climate are simulated with greater fidelity by CCSM3 than
371 CCSM2, there are still significant biases that should be addressed in future generations
372 of CCSM. These systematic errors can be illustrated by comparing the CCSM3 con-
373 trol integration against observations and meteorological analyses for the present-day
374 climate. The time period from the control simulation spans the same interval (years
375 400–500) used in the comparisons against CCSM2 (section 3).

376 a. Representation of major modes of variability

377 *Figure in preparation – more detailed text to follow.*

378 The basic characteristics of the ENSO episodes simulated by CCSM2 and CCSM3
379 are quite similar. Two of the most important properties are the total variance and power
380 spectrum of SST anomalies in the central Pacific. The results for the Nino 3.4 region
381 (5S to 5N, 120W to 170W) are representative of other regions in the tropical Pacific.
382 The total variance for the smoothed monthly anomalies in the Nino 3.4 temperature for
383 CCSM2, CCSM3, and meteorological analysis (Kistler et al. 2001) are XXK, YYK,
384 and ZZK, respectively¹¹. These results show that the SST variability associated with

¹⁰line 350: Do we have evidence of the largest changes being below the mixed layer in CCSM2?

¹¹line 384: What are the Nino 3.4 variances for CCSM2, CCSM3, and the NCEP analysis?

385 ENSO events is similar in CCSM2 and CCSM3. The power spectra of the monthly
 386 SST anomalies are shown in Figure 8. The CCSM3, like CCSM2, tends to produce
 387 ENSOs with a periodicity of approximately two years. The observed ENSOs have a
 388 relatively broad spectrum spanning three to five years. Despite the excessive frequency
 389 of ENSOs in the model, the maximum power in the modeled and observed spectra
 390 agree to within XX%¹².

Figure 8

391 **b. Double ITCZ in the Atlantic and Pacific**

392 Like previous generations of this model, CCSM3 produces a double ITCZ in the tropi-
 393 cal Pacific. The southern Pacific convergence zone (SPCZ) in the observations extends
 394 southeast from the warm pool into the central southern Pacific (Figure 9). In CCSM3,
 395 the SPCZ is replaced by a southern branch of the ITCZ that is nearly zonal in orienta-
 396 tion. The error is particularly evident during JJA; when the real SPCZ is much weaker
 397 and less extensive than the modeled convection south of the equator. The model over-
 398 estimates the local precipitation rate in both branches of the ITCZ by up to 10 mm/day.
 399 The maximum precipitation in the northern half of the warm pool is too intense, and it
 400 is displaced westward by approximately 30 degrees relative to the observed maximum.

Figure 9

401 **c. Biases in continental precipitation and temperature**

402 Although the temperature errors in CCSM3 are smaller than those in CCSM2, there
 403 are are still large biases in the 2m air temperatures for sub-Arctic continental regions
 404 during boreal winter. The temperatures relative to observations (Willmott and Mat-
 405 suura 1995; Willmott and Robeson 1995) during DJF are overestimated by as 10K in
 406 parts of Alaska and northern Eurasia. The mean overestimate for sub-Arctic continen-
 407 tal regions north of 50N during DJF is +3.9K. The magnitude of the local errors are
 408 generally smaller than those in CCSM2 (Kiehl and Gent 2003). In addition, there are
 409 significant deficits in precipitation in the southeast United States, Amazonia, and south-
 410 east Asia throughout the annual cycle (Figure 9). These biases cause dynamic models
 411 of vegetation to produce unrealistic distribution of plant phenotypes in the affected re-
 412 gions (Levis and Bonan 2004). For fixed vegetation, models of the terrestrial carbon
 413 cycle are very sensitive to both temperature and precipitation. Higher temperatures
 414 cause water limitation because of the non-linear response of evaporation. This effect
 415 slows plant growth, leading to higher atmospheric concentrations of CO₂. Higher pre-
 416 cipitation causes both heterotrophic respiration and gross primary production (GPP, the
 417 total amount of energy fixed by all photosynthetic organisms) to increase. It is difficult
 418 to predict the net effect on CO₂ concentration since both processes are highly variable
 419 and their effects on CO₂ have opposite sign. Therefore when there are biases in both
 420 temperature and precipitation, it may be difficult to predict the sign of the change in
 421 atmospheric CO₂. For these reasons, it will be important to reduce these biases in fu-
 422 ture versions of CCSM. The biases in annual-mean precipitation for three regions are
 423 listed in Table 1. The underestimation of rainfall ranges between 24% and 28% for
 424 these areas. In order to improve the fidelity of the dynamic vegetation and terrestrial
 425 carbon models, it will be necessary to reduce these errors in future versions of CCSM.

Table 1

¹²line 390: Fill in the percent diff. between the peak powers in spectra for CCSM3 and analysis.

Table 1: Model precipitation for continental regions

Region	Region Box	Precipitation (mm/day)	Error (mm/day)	% Error (percent)
SE United States	30N–40N, 80W–100W	2.4	–0.75	–24
Amazonia	10S–10N, 60W–80W	4.5	–1.7	–28
SE Asia	10N–30N, 80E–110E	3.1	–1.0	–24

One option to reduce the the positive temperature biases during boreal winter is to use a relationship between snow albedo and equivalent water depth which is more consistent with satellite observations (Oleson et al. 2003).

d. SST biases and related atmospheric issues in western coastal regions

CCSM3 produces sea-surface temperatures for the western coastal regions that are warmer than observed (Figure 2). Experiments with earlier versions of the coupled model suggest that the biases in SSTs are caused by underestimates of surface stress and overestimates of surface insolation (*W. Large and G. Danabasoglu, personal communication*). These experiments also show that the biases in these areas affect the SST and precipitation over large portions of the Atlantic and Pacific basins. The weaker surface stress results in weaker cooling of the ocean mixed layer by Ekman pumping, and the excess insolation results in solar heating through absorption of penetrative sunlight. These biases occur in the oceans adjacent to southern Africa and south America. The CCSM3 is compared in Table 2 against observations and analyses for these two western coastal regions averaged over the annual cycle. The comparison includes estimates of SST (Rayner et al. 2003), surface stress (Kistler et al. 2001), and all-sky and clear-sky insolation denoted by S_{\downarrow} and $S_{\downarrow,e}$, respectively (Zhang et al. 2004). In the coastal region adjacent to South America, there CCSM3 overestimates the SST by 3K. While earlier generations of CCSM overestimated the surface insolation off South America by more than 50 Wm^{-2} in the annual mean, CCSM3 tends to slightly underestimate the surface shortwave flux. The much smaller error in insolation results from several modifications to the cloud parameterizations introduced in CCSM3 (Boville and Etcetera 2004) to address this issue. The observational comparison suggests that the weak surface stress in CCSM3 may still partially explain the 3K error in SST. It should be noted that the surface produced by CCSM3 is stronger than that in CCSM2 by up to 0.1 Nm^2 partly because of the increased resolution in the atmosphere (Hack and Etcetera 2004). The factors leading to the SST biases are examined further in Large et al. (2004).

Table 2

e. The semi-annual SST cycle in the eastern Pacific

CCSM3 produces a fairly strong semi-annual cycle for SST in the eastern tropical Pacific that does occur in the real climate system (Figure 10). The region where this

Figure 10

Table 2: Properties of western coastal ocean regions

Region	Source	SST (K)	Stress Nm^{-2}	S_{\downarrow} Wm^{-2}	$S_{\downarrow,c}$ Wm^{-2}
Africa (20S–5S,5W–5E)	Obs.	23.3	0.065	216.7	296.7
	CCSM3	25.6	0.065	223.5	292.2
S. America (20S–5S,65W–55W)	Obs.	20.3	0.071	214.3	300.4
	CCSM3	23.3	0.057	209.6	296.8

discrepancy is particularly evident lies between 5N to 5S and 110W to 90W. The observational climatology for the seasonal cycle in SST for this region is derived from the Hadley Centre’s sea ice and sea surface temperature (SST) data set, HadISST (Rayner et al. 2003). The annual and regional mean temperature from CCSM3 is 25.5C, and this compares well with the HadISST estimate of 25.2C. However, the simulated and observed seasonal cycles in the regional mean SST are quite different. The annual cycle in SST produced by CCSM3 is 1.7C, or 43% of the observed cycle, and it is shifted in phase approximately 1.4 months later in the year. The semi-annual cycle in SST produced by CCSM3 is 1.6C, which is 220% of the semi-annual cycle in the HadISST data set. In the model, the phase of the semi-annual cycle is displaced by 5.3 months relative to the phase of the annual cycle. In summary, the magnitude of the annual cycle is roughly half that observed while the magnitude of the semi-annual cycle is roughly twice that observed. The causes for these systematic biases in the model physics have not been identified.

f. Underestimation of downwelling shortwave radiation in polar regions

In the Arctic, CCSM3 underestimates the downwelling all-sky shortwave radiation at the surface throughout the annual cycle. The insolation is underestimated relative to in situ observations from the Surface Heat Budget of the Arctic (SHEBA) experiment (Persson et al. 2002) and to estimates from the International Satellite Cloud Climatology Project (ISCCP) (Zhang et al. 2004). For this comparison, the ISCCP data for 1984 to 2000 has been averaged to produce a climatology. Between 70N to 90N, the annual-mean downwelling shortwave fluxes for all-sky conditions are 91 Wm^{-2} from ISCCP and 78 Wm^{-2} from CCSM3. The corresponding annual-mean clear-sky fluxes differ by only -3.9 Wm^{-2} , or -3% . The fluxes during the JJA season are 214 Wm^{-2} from ISCCP and 169 Wm^{-2} from CCSM3. The corresponding JJA-mean clear-sky fluxes differ by only 8.5 Wm^{-2} , or 2.7% . Since the clear-sky fluxes are in good agreement, the underestimate of surface insolation by CCSM3 is caused by an overestimate of the surface shortwave cloud radiative effect. Further analysis will be required to identify the sources of this error in the modeled cloud amount, cloud condensate path, and cloud microphysical properties.

6. Conclusions

A new version of the Community Climate System Model, CCSM3, has been developed and released to the climate community. The improvements in the functionality include the flexibility to simulate climate over a wide range of spatial resolutions with greater fidelity. This paper documents the high resolution version used for international assessments of climate change. The atmosphere and land share a grid for the Eulerian spectral atmospheric dynamics running at T85 truncation. The ocean and sea-ice share a 1-degree grid with a displaced pole in the northern hemisphere.

The atmosphere incorporates new treatments of cloud and ice-phase processes; new dynamical frameworks suitable for modeling atmospheric chemistry; improved parameterizations of the interactions among water vapor, solar radiation, and terrestrial thermal radiation; and a new treatment of the effects of aerosols on solar radiation. The land model includes improvements in land-surface physics to reduce temperature biases and new capabilities to enable simulation of dynamic vegetation and the terrestrial carbon cycle. The ocean model has been enhanced with new infrastructure for studying vertical mixing, a more realistic treatment of solar heating by chlorophyll, and improvements to the representation of the ocean mixed layer. The sea ice model includes improved schemes for the horizontal advection of sea ice and for the exchange of salt with the surrounding ocean. The software has been designed so that CCSM3 is readily portable to a wide variety of computer architectures.

The climate produced by high-resolution CCSM3 shows several significant improvements over the climates produced by previous generations of the model. These include reduced sub-Arctic surface temperature biases during boreal winter, reduced tropical SST biases in the Pacific, and a better representation of the equatorial counter-current in the Pacific. The new atmosphere features smaller global biases in all-sky surface insolation; improved simulation of cloud radiative effects in the storm tracks and during ENSO events; smaller biases in upper tropical tropospheric temperatures (Collins et al. 2004b); and a more realistic surface radiation budget under clear-sky conditions. The sea ice features a much more realistic simulation of the spatial distribution of ice concentration and of ice thickness. The climate is stable over 500 years subject to perpetual present-day boundary conditions.

There are still several aspects that should be improved in future versions of CCSM. These include the periodicity of ENSO and its projections onto sea-level pressure and precipitation; the double ITCZ in the Pacific, and the large precipitation biases in the western Indian Ocean. Other major modes of variability that are not well-simulated include the Madden-Julian oscillation. The errors in continental precipitation and temperatures need to be addressed to facilitate modeling of dynamic vegetation and the terrestrial carbon cycle. While the representation of the surface fluxes in coastal regions west of Africa and South America has improved, there are still significant biases in the coastal SSTs. Reduction in these biases will affect the simulation over large areas of the Pacific and Atlantic basins. Finally, there are still significant errors in the radiative energy budget of polar regions. These affect both the seasonal cycle and the climate feedbacks of sea ice.

Research is underway to diagnose these biases at the process level and to test improvements in physics and dynamics that would improve the simulation fidelity. At

Table 3: Control Integrations using CCSM3

Resolution	Present (years)	1%CO ₂ /yr (years)	2×CO ₂ (years)	4×CO ₂ (years)	1780 (years)	1870 (years)	20 th C (years)
T85_gx1v3	b30.009 (661)	b30.026 (161)	b30.026a (152)	b30.036b (153)	– (0)	b30.020 (235)	b30.030 (8×130)
T42_gx1v3	b30.004 (1001)	b30.025 (214)	b30.025a (301)	b30.025b (301)	b30.100 (499)	b30.043 (302)	– (0)
T31_gx3v5	b30.031 (748)	b30.032 (171)	b30.032a (157)	b30.032b (160)	b30.105 (433)	b30.048 (154)	– (0)

the same time, the model is being extended to include a comprehensive treatment of terrestrial and oceanic biogeochemistry and ecosystem dynamics. Detailed representations of reactive chemistry, photochemistry, and aerosol microphysics have been added to the atmosphere. These developments are the initial steps toward building a more comprehensive model of the entire Earth system that can be applied to climates of the past, present, and future.

A. Control integrations of CCSM3

A comprehensive suite of control experiments have been performed with CCSM3. The output from these experiments has been made available to the climate community and may be used without restriction. Each of the configurations has been integrated using the three standard configurations of CCSM (section a. The experiments include simulations under constant present-day and preindustrial conditions corresponding to 1780 and 1870. In order to characterize the sensitivity of the model to increased atmospheric concentrations of CO₂, the model has been integrated with a 1% increase in CO₂ per year starting from initial conditions obtained from the present-day run. Two other simulations have been branched from the transient 1%CO₂/year simulation when the decadal-mean CO₂ concentration is equal to two times and four times its present-day value. The CO₂ concentration is held fixed in each of these runs to the values at the branch points from the transient simulation. For the purposes of these control experiments, the present-day global-mean annually-averaged mixing-ratio of CO₂ is equal to 355 ppmv, its value in 1990.

The control integrations are shown in Table 3. The table lists the types of experiments, the resolution used in each integration, the length of each experiment in years, and the series identifier for each simulation. For more details regarding the types of model output available and the methods for access to these data, please contact the CCSM3 data working group¹³. The control experiment discussed in this paper is b30.009.

Table 3

¹³line 558: correct?

561 **Acknowledgement** The authors wish to acknowledge members of the CCSM Soft-
562 ware Engineering Group and NCAR's Divisions for Climate and Global Dynamics,
563 Atmospheric Chemistry, and Scientific Computing for their substantial contributions
564 to the development of CCSM3.

565 The new model would not exist without the significant input from members of the
566 CCSM working groups for software engineering and the component models for the
567 atmosphere, land, ocean, and sea-ice too numerous to mention.

568 We would like to acknowledge the substantial contributions to the CCSM project
569 from the National Science Foundation (NSF), Department of Energy (DOE), the Na-
570 tional Oceanic and Atmospheric Administration, and the National Aeronautics and
571 Space Administration.

572 This study is based on model integrations were performed by NCAR and CRIEPI
573 with support and facilities provided by NSF, DOE, MEXT, and ESC/JAMSTEC.

574 **References**

575 Alexander, M. A., G. Branstator, A. Capotondi, C. Cassou, R. I. Cullather, Y.-O. Kwon,
576 J. R. Norris, and I. Wainer, 2004: Extra-tropical coupled ocean-atmosphere variabil-
577 ity. *J. Clim.*, *this issue*.

578 Ammann, C. M., G. A. Meehl, W. M. Washington, and C. S. Zender, 2003: A monthly
579 and latitudinally varying volcanic forcing dataset in simulations of 20th century cli-
580 mate. *Geophys. Res. Lett.*, **30**, 1657, doi:10.1029/2003GL016875.

581 Barth, M. C., P. J. Rasch, J. T. Kiehl, C. M. Benkovitz, and S. E. Schwartz, 2000:
582 Sulfur chemistry in the National Center for Atmospheric Research Community Cli-
583 mate Model: Description, evaluation, features and sensitivity to aqueous chemistry.
584 *J. Geophys. Res.*, **105**, 1387–1415.

585 Bonan, G. B., S. Levis, L. Kergoat, and K. W. Oleson, 2001: Landscapes as patches of
586 plant functional types: An integrating approach for climate and ecosystem models.
587 *Glob. Biogeochem. Cycles*, **16**, 5.1–5.23.

588 Boville, B. A. and Etcetera, 2004: The impact of changing moist physical processes on
589 the general circulation of CAM: Sensitivity studies. *J. Clim.*, *this issue*.

590 Boville, B. A. and P. R. Gent, 1998: The NCAR Climate System Model, Version One.
591 *J. Clim.*, **11**, 1115–1130.

592 Boville, B. A., P. J. Rasch, and Etcetera, 2004: Effect of numerical formulation of FV
593 atmospheric dynamics on the atmospheric general circulation. *J. Clim.*, *this issue*.

594 Briegleb, B. P., C. M. Bitz, E. C. Hunke, W. H. Lipscomb, M. M. Holland, J. L.
595 Schramm, and R. E. Moritz, 2004: Scientific description of the sea ice compo-
596 nent in the Community Climate System Model, Version Three. Technical Report
597 NCAR/TN-463+STR, National Center for Atmospheric Research, Boulder, CO.
598 80307-3000, 78 pp.

- 599 Briegleb, B. P. and D. H. Bromwich, 1998: Polar radiation budgets of the NCAR
600 CCM3. *J. Clim.*, **11**, 1246–1286.
- 601 Collins, W. D., 2001: Parameterization of generalized cloud overlap for radiative cal-
602 culations in general circulation models. *J. Atmos. Sci.*, **58**, 3224–3242.
- 603 Collins, W. D., J. K. Hackney, and D. P. Edwards, 2002a: A new parameterization
604 for infrared emission and absorption by water vapor in the National Center for At-
605 mospheric Research Community Atmosphere Model. *J. Geophys. Res.*, **107**, 8028,
606 doi:10.1029/2000JD000032.
- 607 Collins, W. D., J. M. Lee-Taylor, D. P. Edwards, and G. L. Francis, 2004a: Effects of
608 increased near-infrared absorption by water vapor on the climate system. *J. Geophys.*
609 *Res.*, in preparation.
- 610 Collins, W. D., P. J. Rasch, B. A. Boville, J. J. Hack, J. R. McCaa, D. L. Williamson,
611 B. P. Briegleb, C. M. Bitz, S.-J. Lin, M. H. Zhang, and Y. Dai, 2004b: The formu-
612 lation and atmospheric simulation of the Community Atmosphere Model: CAM3.
613 *J. Clim.*, *this issue*.
- 614 Collins, W. D., P. J. Rasch, B. A. Boville, J. J. Hack, J. R. McCaa, D. L. Williamson,
615 J. T. Kiehl, B. Briegleb, C. Bitz, S.-J. Lin, M. Zhang, and Y. Dai, 2004c: De-
616 scription of the NCAR Community Atmosphere Model (CAM3). Technical Report
617 NCAR/TN-464+STR, National Center for Atmospheric Research, Boulder, Col-
618 orado 80307-3000, 226 pp.
- 619 Collins, W. D., P. J. Rasch, B. E. Eaton, D. W. Fillmore, J. T. Kiehl, T. C. Beck,
620 and C. S. Zender, 2002b: Simulation of aerosol distributions and radiative forc-
621 ing for INDOEX: Regional climate impacts. *J. Geophys. Res.*, **107**, 4664, doi:
622 10.1029/2001JD001365.
- 623 Collins, W. D., P. J. Rasch, B. E. Eaton, B. Khattatov, J.-F. Lamarque, and C. S. Zender,
624 2001: Simulating aerosols using a chemical transport model with assimilation of
625 satellite aerosol retrievals: Methodology for INDOEX. *J. Geophys. Res.*, **106**, 7313–
626 7336.
- 627 Connolley, W. M., J. M. Gregory, E. C. Hunke, and A. J. McLaren, 2004: On the
628 consistent scaling of terms in the sea ice dynamics equation. *J. Phys. Oceanogr.*,
629 1776–1780.
- 630 Deser, C., A. Capotondi, and R. Saravanan, 2004: ENSO and tropical Atlantic vari-
631 ability in CCSM3. *J. Clim.*, *this issue*.
- 632 DeWeaver, E. and C. M. Bitz, 2004: Atmospheric circulation and Arctic sea ice in
633 CCSM3 at medium and high resolutions. *J. Clim.*, *this issue*.
- 634 Gent, P. R., F. Bryan, D. Tsumune, K. Lindsay, G. Danabasoglu, M. Hecht, and S. C.
635 Doney, 2004: Thermocline and deep ocean ventilation during the 20th century in the
636 CCSM3. *J. Clim.*, *this issue*.

- 637 Hack, J. J. and Etcetera, 2004: Impacts of horizontal resolution on ccs3. *J. Clim.*, *this*
638 *issue*.
- 639 Harrison, E. F., P. Minnis, B. R. Barkstrom, V. Ramanathan, R. D. Cess, and G. G.
640 Gibson, 1990: Seasonal variation of cloud radiative forcing derived from the Earth
641 Radiation Budget Experiment. *J. Geophys. Res.*, **95**, 18687–18703.
- 642 Hurrell, J. W. and Etcetera, 2004: Dynamic circulation and variability. *J. Clim.*, *this*
643 *issue*.
- 644 IPCC, 2001: *Climate Change 2001 : The Scientific Basis*. Cambridge University Press,
645 ed., J. T. Houghton, Y. Ding, D. J. Griggs, M. Noguer, P. J. van der Linden, and
646 D. Xiaosu, 944 pp.
- 647 Kiehl, J. T., W. D. Collins, J. J. Hack, and C. Shields, 2004: The climate sensitivity of
648 CCSM3. *J. Clim.*, *this issue*.
- 649 Kiehl, J. T. and P. R. Gent, 2003: The Community Climate System Model, Version
650 Two. *J. Clim.*, **17**, 3666–3682.
- 651 Kiehl, J. T. and K. E. Trenberth, 1997: Earth’s annual global mean energy budget. *Bull.*
652 *Am. Meteorol. Soc.*, **78**, 197–208.
- 653 Kistler, R., E. Kalnay, W. Collins, S. Saha, G. White, J. Woollen, M. Chelliah,
654 W. Ebisuzaki, M. Kanamitsu, V. Kousky, H. van den Dool, R. Jenne, and M. Fior-
655 ino, 2001: The NCEP-NCAR 50-year reanalysis: Monthly means CD-ROM and
656 documentation. *Bull. Am. Meteorol. Soc.*, **82**, 247–267.
- 657 Large, W. G., G. Danabasoglu, and I. Wainer, 2004: Attribution and implications of
658 upper ocean biases in CCSM3. *J. Clim.*, *this issue*.
- 659 Levis, S. and G. B. Bonan, 2004: Evaluation of CLM parameterizations and CAM-
660 CLM climate using the CLM-DGVM as a diagnostic tool. *J. Clim.*, *this issue*.
- 661 Libscomb, W. H. and E. C. Hunke, 2004: Modeling sea-ice transport using incremental
662 remapping. *Mon. Wea. Rev.*, **132**, 1341–1354.
- 663 Lin, S.-J. and R. B. Rood, 1996: Multidimensional flux-form semi-Lagrangian trans-
664 port schemes. *Mon. Wea. Rev.*, **124**, 2046–70.
- 665 — 1997: An explicit flux-form semi-Lagrangian shallow-water model on the sphere.
666 *Q. J. R. Meteorol. Soc.*, **123**, 2477–2498.
- 667 McPhaden, M. J., A. J. Busalacchi, R. Cheney, J. R. Donguy, K. S. Gage, D. Halpern,
668 M. Ji, P. Julian, G. Meyers, G. T. Mitchum, P. P. Niiler, J. Picaut, R. W. Reynolds,
669 N. Smith, and K. Takeuchi, 1998: The tropical ocean global atmosphere observing
670 system: A decade of progress. *J. Geophys. Res.*, **103**, 14169–14240.
- 671 Meehl, G. A., J. M. Arblaster, D. M. Lawrence, E. K. Schneider, and A. Seth, 2004:
672 Monsoon regimes in CCSM3. *J. Clim.*, *this issue*.

- 673 Ohlmann, J. C., 2004: Ocean radiant heating in climate models. *J. Clim.*, **16**, 1337–
674 1351.
- 675 Oleson, K. W., G. B. Bonan, C. Schaaf, F. Gao, Y. Jin, and A. Strahler, 2003: Assess-
676 ment of global climate model land surface albedo using MODIS data. *Geophys. Res.*
677 *Lett.*, **20**, 1443, doi:10.1029/2002GL016749.
- 678 Oleson, K. W., Y. Dai, G. B. Bonan, M. Bosilovich, R. Dickinson, P. Dirmeyer,
679 F. Hoffman, P. Houser, S. Levis, G.-Y. Niu, P. Thornton, M. Vertenstein, Z.-L. Yang,
680 and X. Zeng, 2004: Technical description of the Community Land Model (CLM).
681 Technical Report NCAR/TN-461+STR, National Center for Atmospheric Research,
682 Boulder, CO. 80307-3000, 174 pp.
- 683 Otto-Bliesner, B. L., E. C. Brady, G. Clauzet, Z. Kothavala, S. Levis, and R. A. Tomas,
684 2004: Sensitivity of the climate system to glacial-interglacial forcing in CCSM3.
685 *J. Clim.*, *this issue*.
- 686 Persson, P. O. G., C. W. Fairall, E. L. Andreas, P. S. Guest, and D. K. Perovich, 2002:
687 Measurements near the Atmospheric Surface Flux Group tower at SHEBA: Near-
688 surface conditions and surface energy budget. *J. Geophys. Res.*, **C107**, 8045, doi:
689 10.1029/2000JC000705.
- 690 Rasch, P. J., M. C. Barth, J. T. Kiehl, S. E. Schwartz, and C. M. Benkovitz, 2000: A
691 description of the global sulfur cycle and its controlling processes in the National
692 Center for Atmospheric Research Community Climate Model, Version 3. *J. Geo-*
693 *phys. Res.*, **105**, 1367–1385.
- 694 Rasch, P. J., W. D. Collins, and B. E. Eaton, 2001: Understanding the Indian Ocean Ex-
695 periment (INDOEX) aerosol distributions with an aerosol assimilation. *J. Geophys.*
696 *Res.*, **106**, 7337–7356.
- 697 Rayner, N. A., D. E. Parker, E. B. Horton, C. K. Folland, L. V. Alexander, D. P. Powell,
698 E. C. Kent, and A. Kaplan, 2003: Global analyses of sea surface temperature, sea
699 ice, and night marine air temperature since the late nineteenth century. *J. Geophys.*
700 *Res.*, **108**, 4407, doi:10.1029/2002JD002670.
- 701 Smith, R. D., S. Kortas, and B. Meltz, 1995: Curvilinear coordinates for global ocean
702 models. Technical Report LA-UR-95-1146, Los Alamos National Laboratory.
- 703 Timmermann, R., A. Worby, H. Goosse, and T. Fichefet, 2004: Utilizing the aspect sea
704 ice thickness data set to evaluate a global coupled sea ice-ocean model. *J. Geophys.*
705 *Res.*, **C109**, C07017, doi:10.1029/2003JC002242.
- 706 Weatherly, J. W., B. P. Briegleb, and W. G. Large, 1998: Sea ice and polar climate in
707 the NCAR CSM. *J. Clim.*, **11**, 1472–1486.
- 708 Williamson, D. L., 2002: Time-split versus process-split coupling of parameterizations
709 and dynamical core. *Mon. Wea. Rev.*, **130**, 2024–2041.

- 710 Willmott, C. J. and K. Matsuura, 1995: Smart interpolation of annually averaged air-
711 temperature in the United States. *J. Appl. Meteorol.*, **34**, 2577–2586.
- 712 Willmott, C. J. and S. M. Robeson, 1995: Climatologically aided interpolation (CAI)
713 of terrestrial air-temperature. *International Journal Of Climatology*, **15**, 221–229.
- 714 Yeager, S. G., J. J. Hack, C. Shields, and W. G. Large, 2004: Low resolution CCSM3.
715 *J. Clim., this issue*.
- 716 Zhang, Y. C., W. B. Rossow, A. A. Lacis, V. Oinas, and M. I. Mishchenko, 2004:
717 Calculation of radiative fluxes from the surface to top of atmosphere based on ISCCP
718 and other global data sets: Refinements of the radiative transfer model and the input
719 data. *J. Geophys. Res.*, **109**, D19105, doi:10.1029/2003JD004457.

This work was performed under the auspices of the U.S. Department of Energy by the University of California, Lawrence Livermore National Laboratory under Contract No. W-7405-Eng-48.

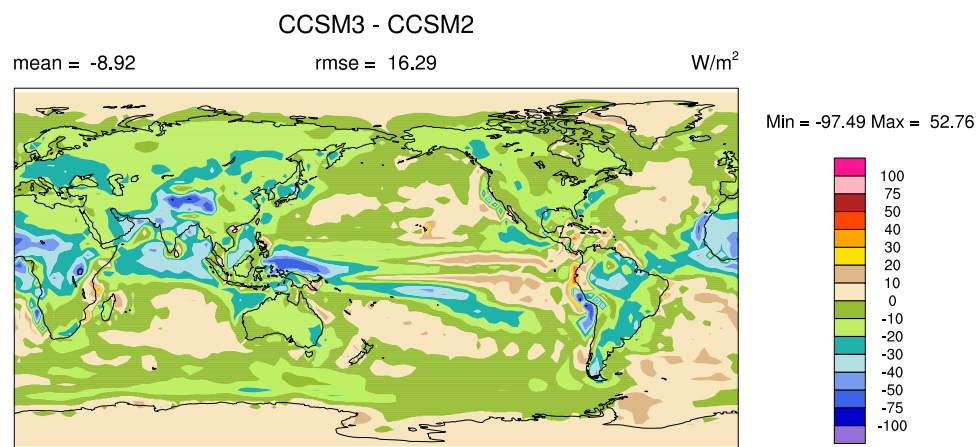


Figure 1: Difference in annual-mean net surface insolation between CCSM2 and CCSM3.

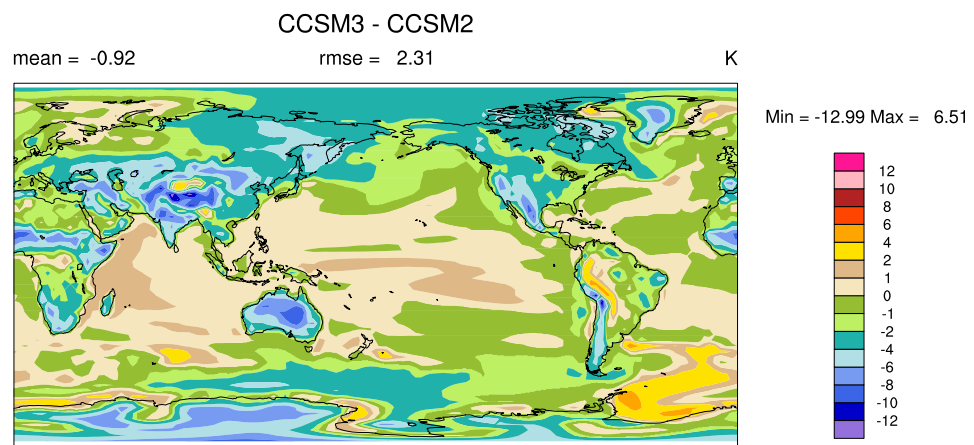


Figure 2: Difference in annual-mean surface temperature between CCSM2 and CCSM3.

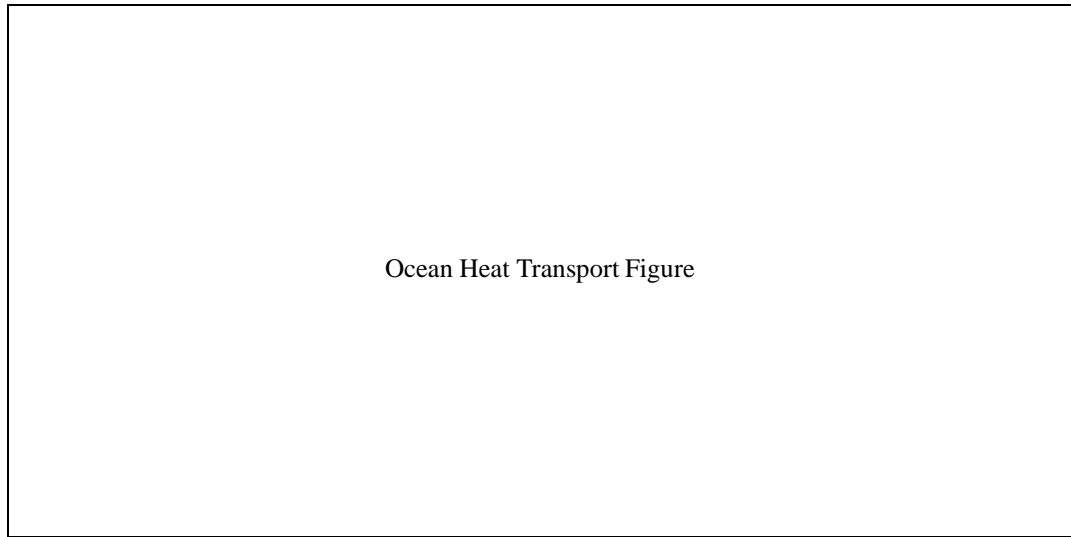


Figure 3: Difference in annual-mean meridional ocean heat transport between CCSM2 and CCSM3.

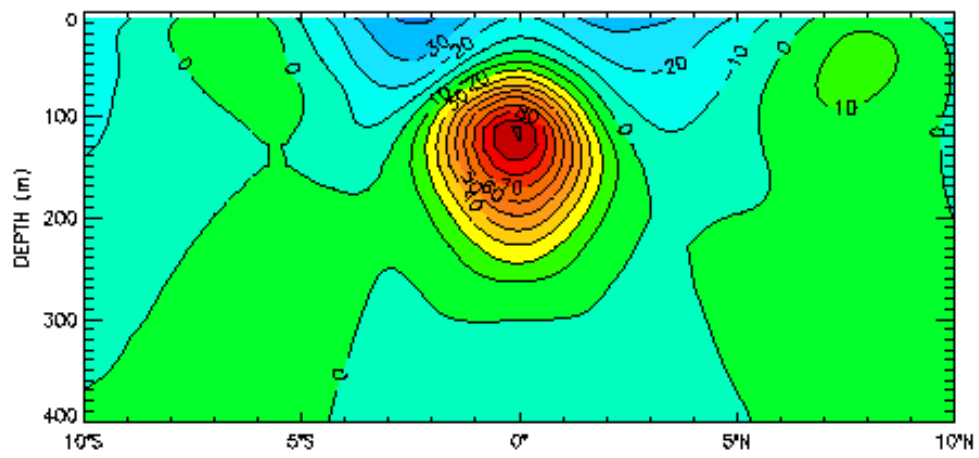


Figure 4: Difference in annual-mean zonal equatorial undercurrent (cm/s) in the Pacific.

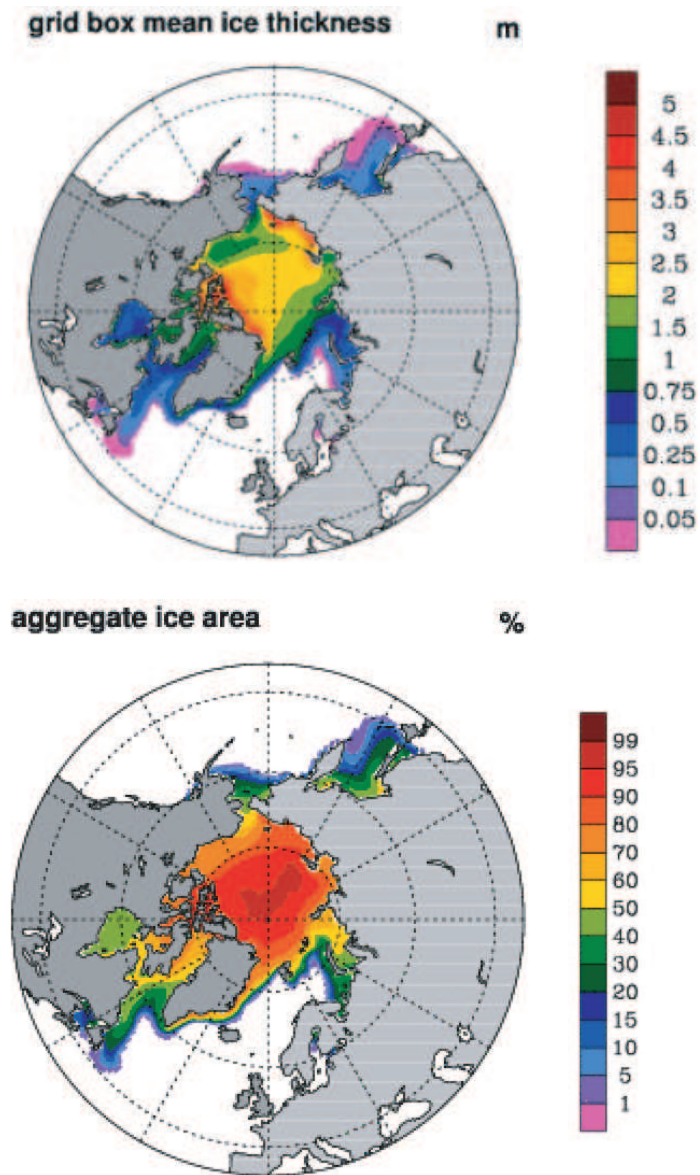


Figure 5: Annual-mean sea-ice thickness and concentration from CCSM3.

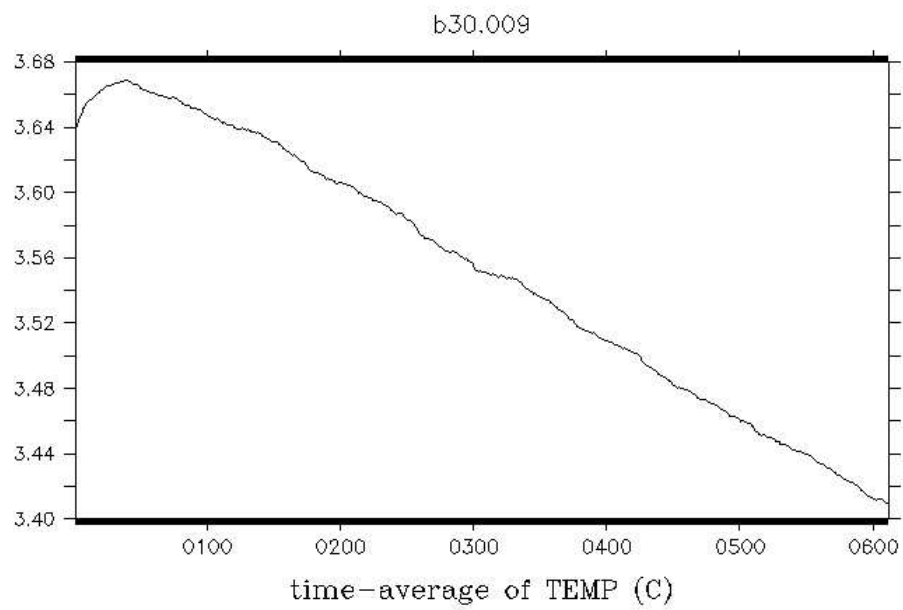


Figure 6: Annual-mean globally-averaged ocean potential temperature as a function of year of simulation.



Vertical X-section of Ocean Pot. Temp. vs Time

Figure 7: Global-mean ocean potential temperature as a function of depth and year of simulation.

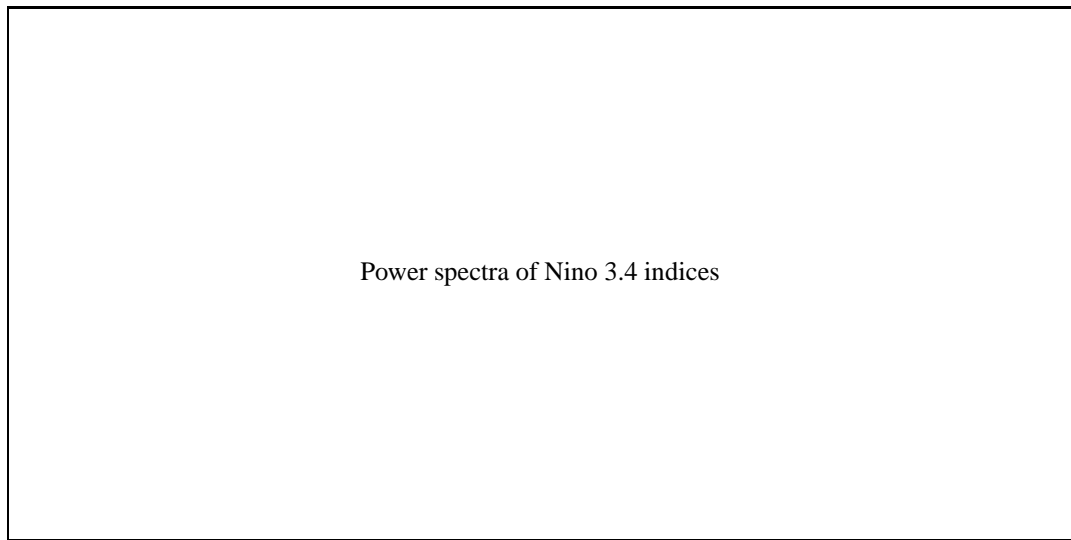


Figure 8: Power spectra of the the Nino 3.4 indices for CCSM2, CCSM3, and the HadiSST(?) data set.

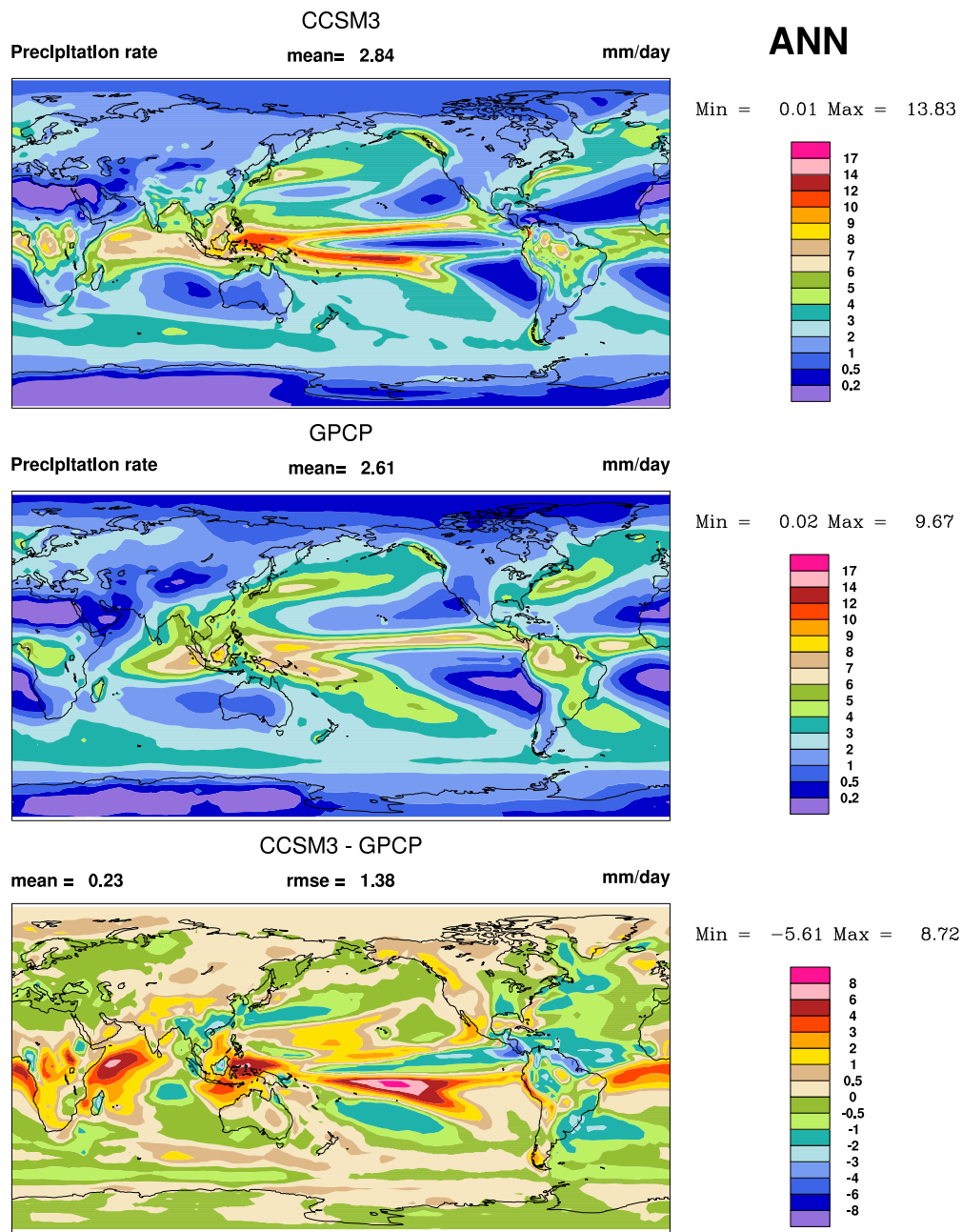


Figure 9: Annual-mean precipitation from CCSM3, the GPCP data set, and the difference between CCSM3 and GPCP.

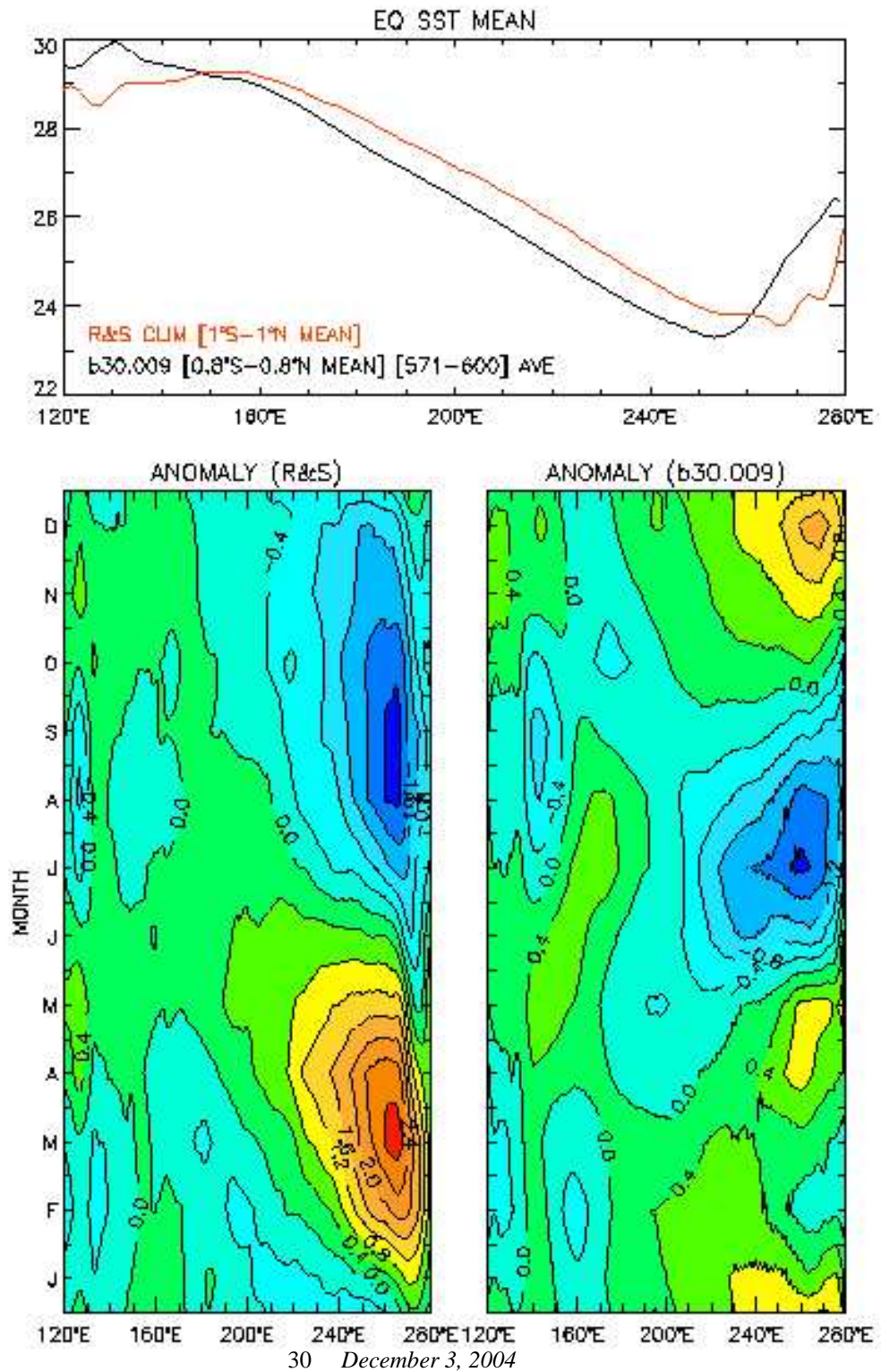


Figure 10: Seasonal cycle in surface temperature anomalies relative to the annual mean for 5S–5N and 120E–80W.